INTERACTION BETWEEN 153-MeV *NEGATIVE PIONS AND HELIUM*

Yu. A. BUDAGOV, P. F. ERMOLOV, E. A. KUSHNIRENKO, and V. I. MOSKALEV

Joint Institute for Nuclear Research

Submitted to JETP editor December 29, 1961

J. Exptl. Theoret. Phys. (U.S.S.R.) **42**, 1191-1208 (May, 1961)

The interaction between 153-MeV π^- mesons and He^4 nuclei was investigated with a high pressure diffusion cloud chamber operating in a magnetic field. The total π^-He interaction cross section, the elastic scattering cross section, and the cross sections for a number of inelastic processes were determined from measurements of the total π^--meson track length in the chamber. The angular distribution of π^-He elastic scattering is of a diffractive nature with a distinct minimum (80°) and a secondary maximum (100°). Optical model calculations under the assumption of a square-well complex potential $V = V_R + iV_I$ show that best agreement with the experimental data can be obtained for parameter values $V_R = -(18 \pm 7)$ MeV and $V_I = -(63 \pm 6)$ MeV, $r_0 = 1.5 \times 10^{-13}$ cm. These values are in good agreement with those computed by Frank, Gammel, and Watson [4] from the relation between the optical potential and the forward scattering amplitude for free πp scattering. The angular distribution for quasi-elastic scattering of π^- mesons on bound nucleons is compared with the calculations of Watson and Zemach. [35] The probability of multiple scattering of pions in the nucleus and the charge-exchange scattering cross section are estimated.

1. INTRODUCTION

THE basic processes occurring in the interactions of pions of several hundred MeV energy with complex nuclei are coherent elastic scattering on the nucleus as a whole, inelastic scattering, and absorption of the pions. Elastic scattering is usually analyzed on the basis of the optical model, [1] whereby we describe the complex process of interaction of the incident pion with the nucleon by introducing into the wave equation some equivalent complex potential $V = V_R \pm iV_I$ depending only on the range of interaction. The imaginary part of the potential takes into account the attenuation of the particle flux caused by inelastic processes. From the solution of this wave equation we can obtain the angular distribution for elastic scattering and the total cross section for all inelastic processes. Inelastic scattering of pions by nuclei is considered to be the result of scattering by independent nucleons inside the nucleus in a potential well V_R which have a certain energy distribution and do not interact with one another (Serber-Goldberger model [2]). Finally, the absorption of pions by nuclei is satisfactorily explained by absorption on pairs of different nucleons inside the nucleus.

Intensive investigations of pion scattering by free protons carried out during the last few years have permitted the calculation of the real and imaginary parts of the optical potential [4] (or the corresponding coefficients of refraction and absorption in nuclear matter [5]) on the basis of data on elementary πN interactions. Detailed calculations by Frank, Gammel, and Watson (FGW) [4] have shown that the energy dependence of the potentials V_R and V_I in the energy region up to 300 MeV is due to the strong pion-nucleon resonance interaction in the $T = 3/2$, $J = 3/2$ state at energies of about 190 MeV. The experimental determination of V_R and V_I at energies close to the resonance is therefore of importance from the viewpoint of obtaining confirmation of the basic concepts of the FGW model.

In the energy interval up to 300 MeV, the interaction of pions with nuclei has been investigated in a number of experiments with the aid of emulsion, [6-10] cloud chambers, [11-13] and bubble chambers. [14-16] These experiments outlined the basic features of the processes occurring in the interaction of pions with complex nuclei, but the conclusions concerning elastic scattering are primarily of a semiqualitative character, owing to the relatively poor statistical accuracy and difficulties of identification. Considerably greater accuracy in the measurements of elastic scattering can be obtained by electronic methods. [17-19] In the experiments of Baker et al [19] it was shown that at pion energies of about 80 MeV very good agreement with

experiment can be obtained on the basis of a modified Kisslinger model [20] taking into account the gradient of the nuclear density at the nuclear boundary. Measurements of the angular distribution for elastic scattering of 150-MeV pions on C, Al, Cu, and Pb nuclei with the use of Cerenkov counters to separate the particles according to their energy and with an amplitude analyzer were made by Fujii. [21] However, owing to the insufficient energy and angular resolution of the arrangement in this experiment, no characteristic diffraction pattern was obtained in the region of angles greater than 40—60°, and the analysis of the angular distribution was therefore carried out only for angles smaller than 40°. The value of V_I determined by Fujii was close to the calculated value, but the depth of the potential well V_R proved to be greater than that which follows from the FGW calculations.

The interaction of pions with helium nuclei was first observed in a diffusion chamber by Fowler et al. [22] They recorded about 100 interactions at three energies: 53 (π^+), 68 (π^-), and 105 (π^-) MeV. Kozodaev et al [23] also investigated elastic and inelastic πHe interactions in a diffusion chamber with 273-MeV π^+ mesons and 330-Mev π^- mesons (550 events at both energies). The cross section for the elastic scattering of π^- mesons in this experiment in the angular region 5—15° (c.m.s.) turned out to be considerably smaller than the corresponding cross section for π^+ mesons. This effect was interpreted by the authors as due to interference between Coulomb and nuclear scattering. Recently, Brautti et al [24] obtained the total π^-He cross section and the angular distribution of π^-He elastic scattering at 0.97, 1.67, 2.26 BeV with the aid of a helium bubble chamber.

In the present article, we present the results of a study of π^--meson interactions with helium nuclei at 153 MeV carried out with the aid of a high pressure diffusion chamber in a magnetic field. The basic aim of this work was to obtain information on the angular distribution of π^-He elastic scattering to an accuracy sufficient for a reliable determination of the optical model parameters and their comparison with the FGW calculations. The choice of such a light nucleus as He^4 for the target nucleus is useful, since, according to FGW, the depth of the potential well should be the same for heavy and light nuclei. In this work, we also obtained the total cross sections and some other characteristics of a number of processes occurring in inelastic π^-He interactions.

2. EXPERIMENTAL ARRANGEMENT

The diffusion chamber and the experimental layout has been described in detail previously. [25]

In our experiment, the magnetic field in the fiducial region of the chamber had the following characteristics: 1) the field intensity at the center of the effective region was 12 000 Oe, 2) the maximum decrease in the field along the radius in the central plane of the fiducial region was 3%, 3) the maximum inhomogeneity at the height of the sensitive volume was ±4%.

The mean meson energy in the chamber was determined by measurements of the radius of curvature of meson tracks on specially selected pictures and turned out to be 153 MeV. With allowance for the experimental accuracy of the radius measurements (~ 3%), we obtain the value of 9 MeV for the half-width of the pion energy distribution in the chamber, The total contamination due to μ^- mesons and electrons in the beam was (16 ± 2)%. [25]

The chamber was filled with ordinary commercial helium to a pressure P_{eff} = 17.6 atm. In a series of exposures, we obtained about 30 000 stereophotographs. Some data obtained during the analysis of these photographs were published earlier. [26]

3. REDUCTION OF EXPERIMENTAL DATA

In the interaction of π^- mesons with He^4 nuclei, the following reactions are possible:

$$\pi^- + He^4 \rightarrow \begin{cases} \pi^- + He^4 & \text{elastic scattering} & (1) \\ \pi^- + He^3 + n & \text{inelastic scattering without charge exchange} & (2) \\ \pi^- + T + p & & (3) \\ \pi^- + (2p + 2n) & & (4) \\ \pi^0 + T + n & \text{inelastic scattering with charge exchange} & (5) \\ \pi^0 + (p + 3n) & & (6) \\ T + n & \text{pion absorption} & (7) \\ (p + 3n) & & (8) \end{cases}$$

Reactions (1) and (2) appear in the pictures as two-prong stars, (3) and (4) appear as three-prong stars and (5)—(8) appear as one-prong stars. In reactions (4), (6), and (8), the nucleons in the parentheses can occur both in the free state and bound in the form of a deuteron.

The scanning yielded 1802 cases of π^-He interactions (660 one-prong, 848 two-prong, and 294 three-prong stars) satisfying certain selection criteria. It was assumed that all these cases involved interactions of pions with helium, since the background from the interaction of pions with complex nuclei of impurities (methyl alcohol) and hydrogen was no greater than 1%. This estimate was made from data obtained during operation of the chamber with hydrogen and a π^--meson beam of similar energy.[25]

To determine the scanning efficiency, we carried out a careful second scan of part of the pictures. If it is assumed that the efficiency for the double scanning was unity, then the efficiencies for recording one-, two-, and three-prong stars were $s_1 = 0.75 \pm 0.02$, $s_2 = 0.88 \pm 0.02$, and $s_3 = 0.90 \pm 0.02$, respectively.

The interactions were analyzed by the reprojection method. For two- and three-prong stars, the coordinates of the point of interaction, the coordinates of points at the middle of the incident pion track and of each prong of the star, the polar angle θ and the azimuthal angle φ of each prong of the star ($\varphi = 0$ corresponds to the case in which the prong lies in the same horizontal plane as the incident pion) were measured directly on the reprojector. The accuracy of the measurements was 0.7° for θ and about 3° for φ. The radii of curvature of the incident-pion and secondary-particle tracks were measured with the aid of a special template. The measurement accuracy of the radii depends on the curvature, length, and direction of the track in space. The mean accuracy of measurement of the radii in our case was 3—4% for a projected track length of 20—25 cm on the horizontal plane and 5—7% for a length of 7—8 cm. In calculating the particle momentum from the measured radius of curvature, we introduced corrections for the inhomogeneity of the magnetic field and the contraction of the bubbles (~ 5%). In those cases in which the secondary heavy particles stopped in the chamber, we measured their ranges and added corrections to take into account the finite width of the track (for ranges < 10 mm), the bubble contraction, and the change in gas density at the height of the fiducial region of the chamber. According to estimates, the error of the energy determination was ≤ 15% for ranges greater than 5 mm.

The identification of reactions (1)—(8) was made as follows. We first selected cases of π^-He elastic scattering from among all two-prong stars. A two-prong star was considered to be an elastic scattering if it satisfied the relation

$$|\,|\varphi_\pi - \varphi_{He}| - 180°\,| < 5° \text{ and } |\theta_{He} - \theta_{He}^{calc}| < 2°, \quad (9)$$

where φ_π, φ_{He}, and θ_{He} are the measured angles, and θ_{He}^{calc} is the calculated He^4 scattering angle determined from the measured angle θ_π with the aid of the usual kinematical relations for elastic scattering. When the heavy particle of a two-prong star stops in the chamber, an additional selection criterion for reaction (1) is the correspondence between the measured and calculated ranges. As a result, it was found that of 848 two-prong stars 521 represented elastic scattering [reaction (1)], while 304 were cases of reaction (2). In the remaining 23 cases, no reliable separation between reactions (1) and (2) could be made.

The identification of three-prong stars is more complex, since among this group, apart from reaction (3) with three charged particles as the reaction products, there is still reaction (4) with the final products

$$\pi^- + d + p + n, \qquad \pi^- + p + p + n + n, \qquad \pi^- + d + d.$$

To separate reaction (3), we made a kinematical analysis of all cases; this analysis involved momentum and energy balances for different assumptions as to the nature of the secondary particles (p, d, or T). In some cases, we used as additional criteria for identification the measurements of the radii of curvature of the secondary particles, the ranges, or track lengths for particles not stopping in the chamber. The kinematical calculations for all three-prong stars were made on a Ural electronic computer. The general features of the identification procedure were similar to those described by Kozodaev et al.[23] It was found that 87 of the 294 three-prong stars could be assigned to reaction* (3), and the remaining stars to reaction (4).

In view of the complexity and uncertainties, no identification of reactions (5)—(8), occurring among the group of one-prong stars, was made. Some information about the probability of inelastic scattering with charge exchange [reactions (5)—(6)] can be obtained from the fact that two events were observed in which the secondary particles are a fast electron and a fast positron with a small angle between them, i.e., a Dalitz pair, and one heavy positive particle. Taking the probability of the $\pi^0 \to e^-$

*A number of cases of the reaction $\pi^- + He^4 \to \pi^- + d + d$, which could not be kinematically separated from reaction (3), might be present among this group. However, taking into account the small binding energy of the deuteron, we can assume that the probability of a reaction with the emission of two deuterons is very small. This is also supported by the results of Kozodaev et al,[23] who did not identify a single reaction of this type.

$+ e^+ + \gamma$ decay [27] equal to 0.0117, we find that approximately one-fourth of the one-prong stars involve inelastic scattering with charge exchange.

4. TOTAL CROSS SECTIONS

The π^-He total cross section and the cross sections for the individual reactions were determined by counting the number of events and the total π^--meson track length in a rectangular region in the central part of the chamber in which the conditions for recording particles [25] were the best. The total cross sections were calculated from the formula

$$\sigma = Mr/Ln_{\text{eff}}\,(1-q)\,s, \qquad (10)$$

where M is the number of cases of a given reaction in the selected region, L = (5.87 ± 0.09) × 10^6 cm is the total π^--meson track length in this region; n_{eff} = (5.20 ± 0.10) × 10^{20} is the number of He^4 nuclei per cm^3 in a sensitive volume with an effective pressure of 17.6 atm and temperature 25°C; q = 0.16 ± 0.02 is the μ^--meson and electron contamination in the beam; r is a coefficient taking into account the scanning loss for events in which charged particles are emitted at angles φ close to 90° and 270°; r_1 = 1.25 ± 0.04 for reaction (1), r_2 = 1.16 ± 0.04 for reaction (2), while r_{3-8} = 1 for the remaining reactions; s is the scanning efficiency.

Table I shows the number of events M for the various reactions and the total cross sections calculated from formula (10). For the cross sections, the table shows the absolute rms error, which contains the statistical errors in M, and the uncertainty in the value of all quantities used for the calculation of the cross sections from formula (10). The parentheses contain the number of events whose identification was not entirely certain. They were not taken into account in the calculation of the cross sections, but the uncertainty introduced by them was taken into account in the errors of the cross sections.

Table II gives a summary of the experimental data on the πHe cross sections in the energy interval 60—2260 MeV. As seen from this table, the energy dependence of the πHe total cross section and of almost all partial cross sections is fundamentally similar to the character of the energy dependence of the cross sections for elementary πN interactions. This dependence appears again in the case of the πd total cross section and, to a lesser degree, in the case of the cross sections of heavier nuclei. [28,14] However, the value of σ_t obtained in our experiment is considerably below the value resulting from the curve of the energy dependence of the πHe total cross section calculated by Brautti et al [24] from the simple formula

$$\sigma_t^{\text{He}} = 2\overline{(\sigma_{\pi^-p} + \sigma_{\pi^+p})},$$

Table I. Cross sections for various reactions in π^-He interactions at 153 MeV

Reaction	(1)	(2)	(3)	(4)	(5)—(8)	(1)—(8)	(2)—(8)
M	150(2)*	104(2)	26	60	155(1)	495	345
σ, mb	95.0±8.4**	53.4±6.1	11.3±2.3	26.0±3.5	80.6±7.2	266±16	171±12

*Number of events for scattering angles $\theta > 15^\circ$ (c.m.s.)

**We have introduced corrections for scattering in the angular interval 0—15° (c.m.s.) and for Coulomb scattering and interference between Coulomb and nuclear scattering for angles greater than 10° (see Sec. 5).

Table II. Summary of cross sections for πHe interactions in the energy interval 60—2260 MeV

Reference	Energy	Particle	σ_t, mb (1)—(8)	σ_e, mb (1)	σ_i, mb (2)—(8)	$\sigma_{in.sc}$, mb (2)—(4)	$\sigma_{exc}+\sigma_{ab}$, mb (5)—(8)	σ_{exc}, mb (5)—(6)	σ_{ab}, mb (7)—(8)
[22]	60	π^+, π^-	89±18	37±12	52	15±18	37±12	22	15
[22]	105	π^-	207±24	74±14	133	51±12	82±12	62	20
present work	153	π^-	266±16	95±8.4	171±12	90.7±6.6	80.6±7.2	~20	~61
[23]	273	π^+	220±20	75±9	145*	84±9	55±8		
[23]	330	π^-	150±15	47±5	103*	66±6	33±4		
[24]	970	π^-	167.4±5.4						
[24]	1670	π^-	140.7±8.1						
[24]	2260	π^-	104.7±1.5						

*The cross sections were calculated as the difference between σ_t and σ_e and can contain a contribution from reactions other than those in groups (2)—(8).

Table III. π^-He elastic scattering differential cross sections

θ° (c.m.s.)	ΔN	$\frac{d\sigma}{d\Omega}$, mb/sr	θ° (c.m.s.)	ΔN	$\frac{d\sigma}{d\Omega}$, mb/sr
20	82	44.6±6.2	100	17	2.23±0,55
30	124	38.8±4.0	110	14	1.84±0,49
40	97	23.2±2.6	120	12	1.60±0.46
50	75	13.7±1.7	130	7	1.21±0.46
60	39	5.60±0.91	140	3	0.72±0,43
70	8	0,98±0.34	150	2	0.69±0.50
80	4	0.47±0.23	167.5	6	1.72±0.76
90	14	1.85±0.49			

in which the total cross sections for elementary πN collisions were averaged over the velocity distribution functions for bound nucleons:

$$P(\beta)d\beta = 3{,}41\exp[-36{,}4\beta^2]d\beta.$$

5. ANGULAR DISTRIBUTION FOR πHe ELASTIC SCATTERING

1. Experimental data. All cases of elastic scattering, recalculated for the c.m.s., were divided into 15 angular intervals of width 10° (scattering events with $155° < \theta < 180°$ were combined into one interval). Cases of scattering with $\theta < 15°$ were not taken into account in the angular distribution, owing to the low scanning efficiency for these angles. The first and second columns of Table III show the angles θ corresponding to the midpoint of the angular interval and the number of cases of scattering ΔN in each interval. To take into account the scanning losses for events whose plane of scattering was close to the vertical, we constructed the distribution of the azimuthal angle φ for the events in the various angular intervals $\Delta\theta$. The efficiency found from these distributions in the interval $\Delta\theta = 50$—$130°$ corresponds to 92% and drops to 63% in the interval $\Delta\theta = 15$—$25°$.

The differential cross sections $d\sigma/d\Omega$ (third column of Table III) were obtained from the angular distribution $\Delta N/\Delta\Omega$ normalized* to the total cross section σ_e (see Table I) with allowance for the dependence of the scanning loss on the angle φ for a given $\Delta\theta$. No corrections for the angular resolution were introduced, since they were no greater than a few per cent. The errors in the cross sections indicated in the table are due mainly to the statistical error and the uncertainty of the corrections introduced.

2. Optical model calculations. Since the obtained angular distribution for elastic scattering reveals a clear diffraction pattern with a distinct first minimum (~ 80°) and a second maximum (~ 100°) characteristic for scattering by a square-well potential, we calculated the angular distribution for the optical model by means of an exact solution of the wave equation with the use of a complex square-well potential $V = V_R + iV_I$ for the region inside the nucleus $r \le R_0 = r_0A^{1/3}$ and a Coulomb potential $V_C = -2e^2/r$ for the region outside the nucleus $r > R_0$. The Klein-Gordon equation for a pion of total energy E

$$\nabla^2\psi + \frac{(E-V)^2 - \mu^2c^4}{\hbar^2c^2}\psi = 0 \qquad (11)$$

has a solution of the form

$$\psi(r, \theta) = \sum_l \frac{u_l(r)}{r} P_l(\cos\theta). \qquad (12)$$

The radial wave function $u_l(r)$ for the outer region ($r \le R_0$, $V = V_R + iV_I$) satisfies the equation

$$d^2u_l/dr^2 + [k'^2 - l(l+1)/r^2]\,u_l = 0, \qquad (13)$$

where k′ is the wave number inside the nucleus:

$$k'^2 = k_0^2 + (V_R^2 - V_I^2 - 2EV_R)/\hbar^2c^2 + i(2V_RV_I - 2EV_I)/\hbar^2c^2 \equiv a + ib, \qquad (14)$$

$$k' = (a^2+b^2)^{1/4}\left[\cos\left(\tfrac{1}{2}\operatorname{arctg}\tfrac{b}{a}\right) + i\sin\left(\tfrac{1}{2}\operatorname{arctg}\tfrac{b}{a}\right)\right], \qquad (15)^*$$

and k_0 is the wave number of a free pion with a total energy E:

$$k_0^2 = (E^2 - \mu^2c^4)/\hbar^2c^2. \qquad (16)$$

The nonsingular solution of the radial equation (13) at the point r = 0 is expressed in terms of the spherical Bessel function of a complex argument $j_l(k'r)$:

$$u_l(r) = A(k'r)\, j_l(k'r), \qquad (17)$$

connected by the relation

$$j_l(k'r) = (\pi/k'r)^{1/2}J_{l+1/2}(k'r) \qquad (18)$$

with the ordinary Bessel function of half-integral order. Since there are no tables of Bessel func-

*The total cross sections σ_e were not corrected here for Coulomb scattering and for elastic scattering in the angular interval 0–15°.

*arctg = $\tan^{-1}$.

tions of complex arguments, we found the solution of (17) by using the recursion relations [29]

$$\xi_l(x) = \frac{x^2 - l^2 + lx\xi_{l-1}(x)}{lx - x^2\xi_{l-1}(x)} \qquad (19)$$

with the zero-order term

$$\xi_0(x) = \frac{\sin 2y - i \operatorname{sh} 2z}{\operatorname{ch} 2z - \cos 2y} \qquad (20)^*$$

for the function

$$\xi_l(x) = \frac{d}{dx} \ln [x j_l(x)], \qquad (21)$$

which, as is readily seen, is the logarithmic derivative of the radial wave function $u_l(r)$. In formulas (19)—(21), the argument of the function ξ_l is $x = k'r = y + iz$.

The radial wave equation for the region outside the nucleus ($r > R_0$, $V = V_C = -2e^2/r$) has the form

$$d^2u_l^c/dr^2 + [k_0^2 - 2n_c k_0/r - l(l+1)/r^2]\, u_l^c = 0. \qquad (22)$$

In Eq. (22), the quadratic term V_C^2 was not taken into account because of its smallness; n_c represents the Coulomb parameter: $n_c = -2e^2/\hbar v = -2\alpha/\beta$ ($\alpha = 1/137$). For 153-MeV pions, we have $\beta = 0.863$ and $n_c = -0.0169$. The solution of Eq. (22) is a linear combination of the nonsingular solution F_l and the solution G_l which has a singularity at the point $r = 0$: [30]

$$u_l^c = F_l + [G_l + iF_l]\, e^{i\delta_l} \sin \delta_l. \qquad (23)$$

The functions $F_l = F_l(n_c, k_0 r)$ and $G_l = G_l(n_c, k_0 r)$ represent the nonsingular and singular confluent hypergeometric functions.

The complex phase shifts δ_l were found by equating the logarithmic derivatives of the outer (23) and inner (17) solutions at the nuclear boundary $r = R_0$:

$$\frac{[u_l^c(n_c, k_0R_0)]'}{u_l^c(n_c, k_0R_0)} = \frac{k'}{k_0}\xi_l(k'R_0) \equiv g_l. \qquad (24)$$

We thus obtain the equation for the phase shifts δ_l:

$$e^{2i\delta_l} - 1 = \frac{2[F_l'(n_c, k_0R_0) - F_l(n_c, k_0R_0)\, g_l]}{[F_l(n_c, k_0R_0) - iG_l(n_c, k_0R_0)]\, g_l - F_l'(n_c, k_0R_0) + iG_l'(n_c, k_0R_0)}. \qquad (25)$$

Knowledge of the phase shifts δ_l permits the calculation of the differential and total elastic scattering cross sections and the total cross section for all inelastic processes according to the well-known formulas

$$\sigma(\theta) = |f^c(\theta) + f(\theta)|^2$$

$$= \left| -\frac{n_c}{k_0(1-\cos\theta)} \exp\left\{-in_c \ln\left[\frac{1}{2}(1-\cos\theta)\right] + i2\eta_0\right\} + \frac{1}{2ik_0}\sum_l (2l+1)\, e^{2i\eta_l}(e^{2i\delta_l} - 1)\, P_l(\cos\theta)\right|^2, \qquad (26)$$

$$\sigma_i = \pi k_0^{-2} \sum_l (2l+1)\, |e^{2i\delta_l} - 1|^2, \qquad (27)$$

$$\sigma_t = \pi k_0^{-2} \sum_l (2l+1)\, (1 - |e^{2i\delta_l}|^2), \qquad (28)$$

where

$$f^c(\theta) = f_r^c(\theta) + if_i^c(\theta), \qquad f(\theta) = f_r(\theta) + if_i(\theta)$$

are the Coulomb and nuclear scattering amplitudes; $\eta_l = \arg\Gamma(1 + l + in_c)$.

The differential cross section (26) was calculated numerically on a BÉSM electronic computer every 2.5° in the angular interval 5—180°. For four values of the radius: $r_0 = 1.5$, $r_0 = \hbar/\mu c = 1.414$, $r_0 = 1.2$, and $r_0 = 1.0$ (in units of 10^{-13} cm), we calculated about 240 values of $\sigma(\theta)$ for various values of V_R and V_I lying in the intervals 5 MeV $\leq |V_R| \leq$ 50 MeV and 20 Mev $\leq |V_I| <$ 90 MeV. Since in our case $k_0R_0 = 2.89$ for $r_0 = 1.5$, the calculation was carried out for values of l equal to 0, 1, 2, and 3. To check the influence of the phase shift δ_4, part of the calculations was also made with δ_4 taken into account.

The Coulomb wave functions F_l and G_l and their derivatives F_l' and G_l' occurring in Eq. (25) were calculated with the aid of tables [31] by extrapolation of the functions of positive values of n_c for which the values were tabulated to $n_c = -0.0169$. In those cases in which the functions were tabulated to $n_c = 0$, the error in the extrapolation was less than 1%. In the extrapolation from the values $n_c = 0.1585$, the error did not exceed 2—3%.

Along with the cross sections (26)—(28), we also calculated in each variant the mean free path λ for pions in nuclear matter:

$$\lambda = [2(\sqrt{a^2 + b^2} - a)]^{-1/2} = \left[2(a^2 + b^2)^{1/4} \sin\left(\frac{1}{2}\operatorname{arc\,tg}\frac{b}{a}\right)\right]^{-1}, \qquad (29)$$

connected with a complex refractive index of nuclear matter ν by the relation

$$\nu = k'/k_0 = \nu_0 + i(2k_0\lambda)^{-1}, \qquad (30)$$

and the angular dependence of the cross section

*sh = sinh, ch = cosh.

due to the Coulomb interaction:

$$\sigma^c(\theta) = [f_r^c(\theta)]^2 + [f_i^c(\theta)]^2 + 2f_r^c(\theta) f_r(\theta) + 2f_i^c(\theta) f_i(\theta). \quad (31)$$

3. Comparison with experimental results. In order to find the quantities V_R, V_I, and r_0 best describing the experimental angular distribution for elastic scattering $\sigma^{expt}(\theta)$ and the total inelastic cross section σ_i^{expt}, we calculated for each variant the parameter χ^2

$$\chi^2 = \sum_{m=1}^{m=15} \left[\frac{\sigma^{calc}(\theta_m) - \sigma^{expt}(\theta_m)}{\Delta\sigma^{expt}(\theta_m)}\right]^2 + \frac{(\sigma_i^{calc} - \sigma_i^{expt})^2}{(\Delta\sigma_i^{expt})^2}, \quad (32)$$

where $\Delta\sigma$ denotes the experimental errors in the cross sections. The change in the value of χ^2 in the plane (V_R, V_I) for $r_0 = 1.5$ is shown in Fig. 1.

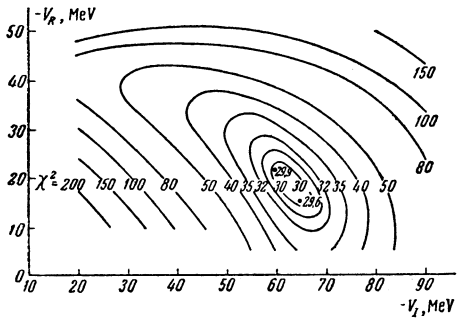

FIG. 1. Distribution of χ^2 in the plane (V_R, V_I) for $r_0 = 1.5$.

As seen from the figure, the χ^2 distribution in this case has a distinct minimum $\chi^2 \approx 30$ in the region $V_R = -(15-20)$ MeV and $V_I = -(60-65)$ MeV. The minimum value χ^2_{min} is 29.6 for $V_R = -15$ MeV, $V_I = -65$ MeV ($\sigma_e^{calc} = 97.2 \times 10^{-27}$ cm^2, $\sigma_i^{calc} = 177 \times 10^{-27}$ cm^2, $\lambda = 1.28 \times 10^{-13}$ cm). For $r_0 = 1.414$, the minimum in the χ^2 distribution is much broader, but less marked, and $\chi^2_{min} \approx 50$. For $r_0 = 1.2$ and $r_0 = 1.0$, χ^2_{min} attains the values 150—300. Hence, we can conclude from the analysis of the χ^2 distribution that the values of the parameters for which we obtain the best agreement with experiment is $r_0 = 1.5$,* $V_R = -18 \pm 7$ MeV, $V = -63 \pm 6$ MeV.†

Figures 2, 3, and 4 illustrate the character of the change in the angular distribution for a variation of the parameters r_0, V_R, and V_I. As seen from these figures, the calculated curve with the parameters $r_0 = 1.5$, $V_R = -20$ MeV, and $V_I = -60$ MeV ($\chi^2 = 29.9$, $\sigma_e^{calc} = 94.1 \times 10^{-27}$ cm^2, $\sigma_i^{calc} = 178 \times 10^{-27}$ cm^2) practically does not differ from the curve with $\chi^2_{min} = 29.6$ and correctly gives the character of the experimental angular distribution. In the angular region up to the first diffraction minimum ($\theta < 80°$), we observe very good agreement between the calculated and experimental distributions, and only in the region of the second maximum does the difference somewhat exceed two standard deviations. If in the calculations we consider only the region of the first diffraction maximum (the first 7 experimental points of the angular distribution), then for $r_0 = 1.5$, we observe a minimum in χ^2 ($\chi^2_{min} = 6$) for close values of the potentials $V_R = -25 \pm 8$ MeV and $V_I = -50 \pm 10$ MeV.

Calculations which include the phase shift δ_4 show that its contribution to the total elastic scattering cross section does not exceed 1% and its

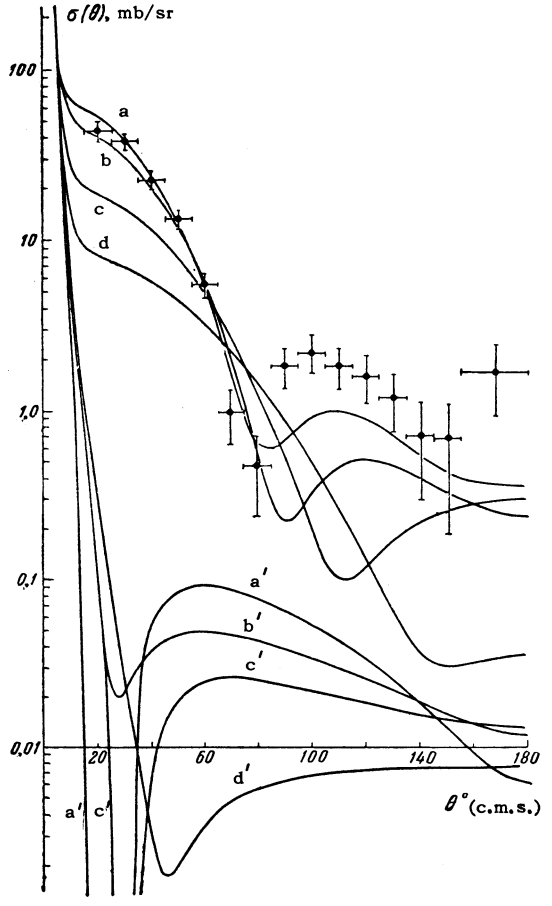

FIG. 2. Change in the angular distribution of π^-He elastic scattering $\sigma(\theta)$ (formula 26) for a variation of the interaction range: a) $r_0 = 1.5$, b) $r_0 = 1.414$, c) $r_0 = 1.2$, d) $r_0 = 1.0$ ($V_R = -20$ MeV, $V_I = -60$ MeV). Curves a′, b′, c′ and d′ represent the angular dependence of the cross section due to the Coulomb interaction $\sigma^c(\theta)$ (formula 31) for the same values of the parameters r_0, V_R, and V_I.

*It should be noted that the value of r_0 characterizes the radius of the potential well rather than the radius of the nucleus and can be somewhat greater than the latter.

†The errors in the potentials shown here do not take into account the clear correlation between V_R and V_I.

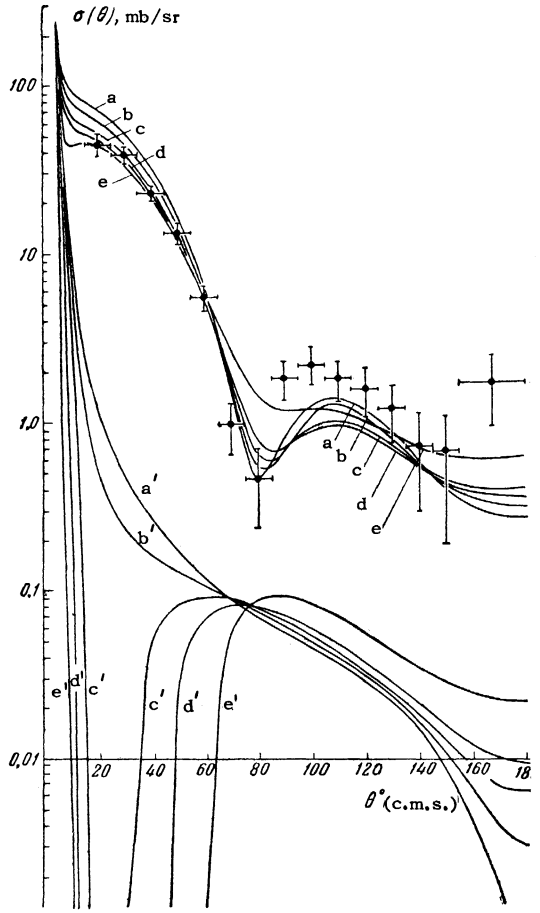

FIG. 3. Change in the angular distribution of π^-He elastic scattering for a variation of the real part of the potential: a) $V_R = -40$ MeV, b) $V_R = -30$ MeV, c) $V_R = -20$ MeV, d) $V_R = -10$ MeV, and e) $V_R = +20$ MeV ($r_0 = 1.5$, $V_I = -60$ MeV). Curves a′, b′, c′, d′, and e′ represent the angular dependence of $\sigma^c(\theta)$ for the same values of the parameters.

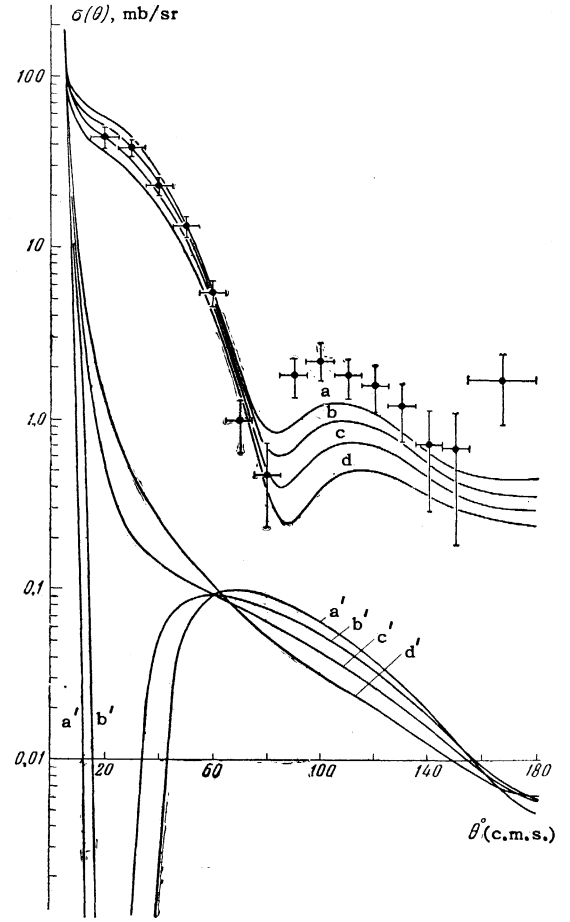

FIG. 4. Change in the angular distribution of π^-He elastic scattering for a variation of the imaginary part of the potential: a) $V_I = -70$ MeV, b) $V_I = -60$ MeV, c) $V_I = -50$ MeV, and d) $V_I = -40$ MeV ($r_0 = 1.5$, $V_R = -20$ MeV). Curves a′, b′, c′, and d′ represent the angular dependence of $\sigma^c(\theta)$ for the same values of the parameters.

influence on the angular distribution in the region of large angles does not lead to better agreement with experiment.

It can be shown that better agreement in the region of the second maximum can be obtained if the model with a square-well potential is modified by the addition of a potential term proportional to the gradient of the nuclear density at the boundary of the nucleus (Kisslinger model [20] and the modified Kisslinger model [19]) or with the use of a potential with a diffuse boundary (for example, the Woods-Saxon potential [32]). In both cases, it is necessary to introduce additional parameters describing the conditions at the nuclear boundary. Although Kisslinger's model is not directly applicable at an energy of about 150 MeV, [19,20] we made a formal attempt to estimate the effect that the addition of a term in the potential proportional to $\nabla\rho\nabla\psi$ would have on the angular distribution. This term leads to a new condition for matching the logarithmic derivatives at the nuclear boundary, [20] which, in our case, has the form

$$\frac{[u_l^c(n_c, k_0R_0)]'}{u_l^c(n_c, k_0R_0)} = \frac{1-w}{k_0R_0} + w\frac{k'}{k_0}\xi_l(k'R_0) \equiv g_l, \qquad (33)$$

where w is a parameter [$w \leq 1$; for $w = 1$, condition (33) goes over to (24)].

For $w = 0.75$ and $w = 0.5$, we calculated about 100 angular distributions with various values of r_0, V_R, and V_I. The best agreement with experiment was obtained for $w = 0.75$, $r_0 = 1.5$, $V_R = -20$ MeV, and $V_I = -70$ MeV ($\chi^2_{min} = 27$). Figure 5 shows the change in the angular distribution for a variation of the parameter w with $r_0 = 1.5$, $V_R = -20$ MeV, and $V_I = -60$ MeV. For other values of r_0 and $w = 0.5$, agreement with experiment was very poor. Thus, independently of the introduction of an additional parameter, we were unable to obtain much better agreement with experiment.

A potential of the Woods-Saxon type or any other form with a diffuse boundary was not used

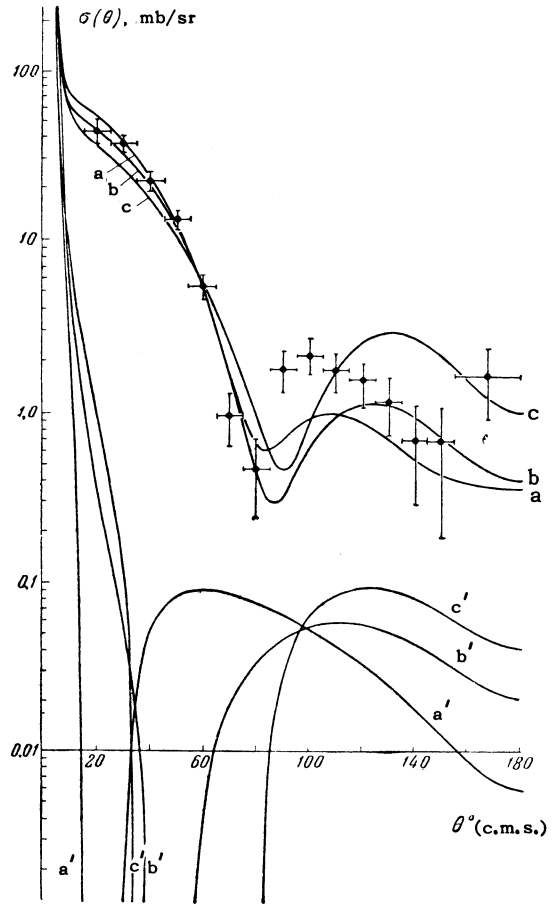

FIG. 5. Change in the angular distribution of π^-He elastic scattering for a variation of the parameter w: a) w = 1, b) w = 0.75, and c) w = 0.5 (r_0 = 1.5, V_R = −20 MeV, V_I = −60 MeV). Curves a′, b′, and c′ represent the angular dependence $\sigma^C(\theta)$ for the same values of the parameters.

in the present experiment in view of the great difficulty of such calculations. It should be noted, however, that an increase in the diffuseness parameter of the Woods-Saxon potential leads to a decrease in the cross section at larger angles in comparison with the square-well potential [32,19] and, hence, scarcely any improvement in the agreement in our case.

The distributions of $\sigma^C(\theta)$ shown in Figs. 2—4 indicate that the Coulomb scattering and the interference effects are important only for angles $\theta < 15°$. Although the angular interval $\theta < 15°$ was not included in this experiment, comparison of the values of $\chi^2 = 29.9$ for $V_R = -20$ MeV, and $\chi^2 = 64.3$ for $V_R = +20$ MeV (curves c and e of Fig. 3) confirms the negative sign of the real part of the potential at energies below resonance. The distribution of $\sigma^C(\theta)$ for $r_0 = 1.5$, $V_R = -20$ MeV, and $V_I = -60$ MeV was used to obtain corrections to the total elastic scattering cross section σ_e in order to take into account Coulomb scattering in the angular interval 15—180° (Table I). Similarly, integration of the dependence $\sigma^n(\theta) = \sigma(\theta) - \sigma^C(\theta)$ in the angular region 0—15° gives a correction to σ_e which takes into account elastic scattering in this angular interval.

4. Discussion. On the basis of general quantum mechanical principles, the optical potential $V(\epsilon)$ can be expressed in terms of the forward scattering amplitude for free pion-nucleon scattering $f_0(\epsilon)$ (averaged over all protons and neutrons of the nucleus):

$$V(\varepsilon) = -(2\pi\hbar v A/k)\,\rho f_0(\varepsilon), \qquad (34)$$

where ρ is the nucleon density in the nucleus, k and v are the pion wave number and velocity, A is the number of nucleons in the nucleus, ϵ is the energy at which the pions are scattered inside the nucleus.

Recent experimental studies of the scattering of pions by free nucleons permit the calculation of $f_0(\epsilon)$ and, consequently, also the optical potential $V(\epsilon)$. In fact, Re $f_0(\epsilon)$ can be calculated from the known phase shifts or from the dispersion relations [33] for pion-nucleon scattering, while Im $f_0(\epsilon)$ can be calculated from the πN total cross section with the use of the optical theorem: Im $f_0(\epsilon) = k\sigma_{\pi N}/4\pi$. A basic assumption of such an approach is the neglect of the multi-particle forces inside the nucleus. Frank, Gammel, and Watson, [4] in the calculation of $V(\epsilon)$, took into account the influence of the Pauli principle, which decreases the total cross section $\sigma_{\pi N}$ in the computation of Im $f_0(\epsilon)$, and introduced into the imaginary part of the potential an additional term taking into account the absorption of pions by pairs of nucleons. [3] Figure 6 shows the FGW calculated curves for the real and imaginary parts of the potential as a function of the pion energy inside the nucleus (dashed curves). The solid curves represent the same dependence recalculated for a pion l.s. kinetic energy ϵ_0 in accordance with the relation $\epsilon_0 = \epsilon + V_R(\epsilon)$. The points in Fig. 6 denote the experimental results of: 1) Shapiro [12] for $C^{12}(\pi^-$, 48 MeV), 2) Byfield et al [11] for $C^{12}(\pi^-$, 62 MeV), 3) Williams et al [19] for Cu($\pi^\pm$, 78 MeV), 4) Pevsner et al [19] for Al ($\pi^\pm$, 80 MeV), 5) Allen et al [10] for emulsion (π^-, 88 MeV), 6) Kessler and Lederman [11] for C^{12} and Pb (π^-, 125 MeV), 7) Fujii [21] for C^{12} (π^-, 150 MeV), 9) Nikol'skiĭ et al [9] for emulsion (π^-, 160 MeV), and 10) Dzhelepov et al [13] for C^{12} (π^-, 230 MeV). The black circles (8) at 153 MeV represent the data of the present experiment for He^4. As seen from the figure, they are in very good agreement with the FGW calculated curves.

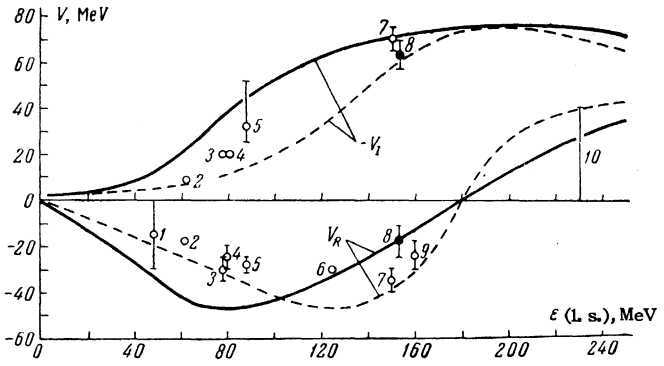

FIG. 6. Energy dependence of the real and imaginary parts V_R and V_I of the optical potential calculated by FGW[4] (the dashed curves are functions of the $\pi^{\pm}$-meson energy inside the nucleus, the solid curves are functions of the pion l.s. energy). The points represent the experimental data of a number of authors (see text).

Correspondingly, we obtain for the mean free path in nuclear matter the value $(1.28-1.40) \times 10^{-13}$ cm, which is in agreement with the value $\lambda/(\hbar/\mu c) \approx 1$ calculated by FGW.

Agreement between the experimental and theoretical values of V_R and V_I for He^4 indicates the suitability of the optical model viewpoint even for such a light nucleus as He^4. On the other hand, it confirms the correctness of the basic assumptions of the FGW model, in particular, the assumptions that the multi-particle forces play a small role in the interaction between pions and bound nucleons and that the depth of the potential well is independent of the nuclear dimensions. Also important is the confirmation of the considerable effect of the strong pion-nucleon interaction close to the resonance energy (maximum of V_I and the passage of V_R through zero at the resonance energy) on the elastic scattering of pions by nuclei. Good agreement between the experimental and theoretical values of the potential also indicates that the effects considered by FGW such as the influence of the momentum distribution of the nucleons in the nucleus, the spatial correlations of the nucleons inside the nucleus, the uncertainty of the pion energy between two successive collisions with nucleons inside the nucleus apparently do not play an important role in scattering.

6. INELASTIC INTERACTIONS OF π^- MESONS WITH HELIUM NUCLEI

Among the inelastic processes (2)—(8), of greatest interest are reactions (2) and (3), which can be interpreted as quasi-elastic scattering of π^- mesons on a bound neutron (2) and a bound proton (3). This interest is due to the possibility of comparing the quasi-elastic scattering of pions on nucleons inside the nucleus and elastic scattering on free protons in order to see whether their properties are identical or different.

The total cross sections for reactions (2) and (3) are shown in Table I. Their comparison indicates that, as in the case of pion energies of the order 300 MeV,[23] the relative probabilities for the scattering of 153-MeV π^- mesons on bound nucleons is less than for free protons at $\pi^{\pm}$-meson energies of 150—170 MeV:[34]

$$\sigma_2/\sigma_3 = 4.7, \qquad \sigma_{\pi^+p}/\sigma_{\pi^-p} = 8.2 - 8.4.$$

The angular distributions $\sigma_2(\theta)$ and $\sigma_3(\theta)$ for reactions (2) and (3) and the angular distribution of all inelastic scatterings of π^- mesons $\sigma_{\text{in. sc}}(\theta)$ [reactions (2)—(4)] are shown in Table IV. The errors shown there take into account mainly the statistical error and a small uncertainty in the correction for the scanning losses due to unfavorable angles φ [for $\sigma_2(\theta)$].

In Figs. 7 and 8, the angular distributions $\sigma_2(\theta)$, $\sigma_3(\theta)$, and $\sigma_{\text{in. sc}}(\theta)$ are compared with the l.s. differential cross sections $\sigma_{\pi^+p}(\theta)$, $\sigma_{\pi^-p}(\theta)$, and $\sigma_{\pi^+p}(\theta) + \sigma_{\pi^-p}(\theta)$, respectively, for scattering on a free proton[34] at an energy $\epsilon = \epsilon_0 - V_R(\epsilon) \approx 170$ MeV. Since the total cross sections for reactions (2)—(4) are one-fourth to one-fifth of the corresponding cross sections for scattering on a free proton (which can be explained by the influence of such factors as the momentum distribution of

Table IV. Angular distribution of inelastically scattered π^- mesons

θ° (l.s.)	$\sigma_2(\theta)$ mb/sr	$\sigma_3(\theta)$, mb/sr	$\sigma_{2-4}(\theta) = \sigma_{in.sc}(\theta)$, mb/sr
30±10	3.58±0.72	1.07±0.36	5.87±0.90
50±10	4.58±0.66	1.24±0.31	6.88±0.77
70±10	3.60±0.57	0.70±0.21	6.41±0.67
90±10	3.64±0.55	1.13±0.26	6.11±0.64
110±10	5.09±0.68	0.82±0.23	8.95±0.80
130±10	5.26±0.79	1.17±0.30	9.23±0.90
150±10		0.48±0.24	7.63±1.00
155±15	4.57±0.86		
170±10			8.56±1.82

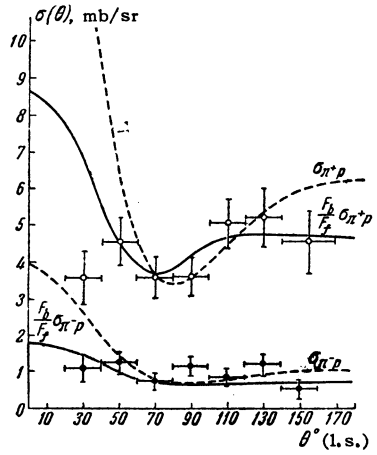

FIG. 7. Angular distributions of π^--mesons from reactions (2) (open circles) and (3) (black circles) in the l.s. The dashed curves are the angular distributions for free π^+p and π^-p scattering at 170 MeV (in arbitrary units), the solid curves are the same distributions multiplied by the Watson-Zemach factor F_b/F_f (in arbitrary units).

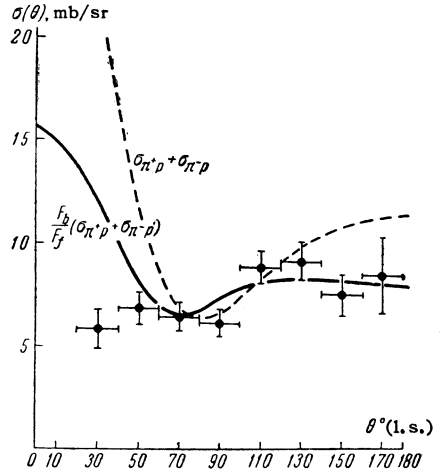

FIG. 8. Angular distribution for inelastically scattered π^- mesons [reactions (2)–(4)] in the l.s. The dashed curve is the angular distribution of the quantity $\sigma_{\pi+p} + \sigma_{\pi-p}$, the solid curve is the quantity $(F_b/F_f)(\sigma_{\pi+p} + \sigma_{\pi-p})$ (in arbitrary units).

the nucleons in the nucleus, screening, etc.), the angular distributions for scattering on free protons are shown on an arbitrary scale (dashed curves). The solid curves represent the angular distributions for scattering on free protons multiplied by the factor of Watson and Zemach [35] F_b/F_f (also in arbitrary units). This factor takes into account approximately the change in the kinematical relations for scattering of pions on bound nucleons due to the presence of the nuclear potential dependent on the pion energy. The angular dependence of the factor F_b/F_f was calculated for a potential $V_R = -18$ MeV found in Sec. 5.

Comparison of the angular distributions of Figs. 7 and 8 indicates that the angular distributions of pions from reactions (2)—(4) basically resemble the angular distributions for free πN scattering. An essential difference observed only at small angles is, perhaps, due to the fact that small momentum transfers to bound nucleons are forbidden by the Pauli principle. It should be noted that, despite the roughness of the approximation used by Watson and Zemach, their calculations give a qualitatively correct description of the character of the change in the angular distribution due to the influence of the nucleus.

The momentum spectra of π^- mesons from reactions (2) and (3) have been given in an earlier publication. [26] The mean energies of these spectra favor the one-nucleon character of the interaction between π^- mesons and the nucleus.

The reactions in group (4) can arise as a result of quasi-elastic scattering of a π^- meson on a bound nucleon with a subsequent nucleon cascade in the nucleus as a result of successive collisions of the π^- meson with several nucleons in the nucleus and also in a collective interaction with a group of nucleons. Using the terminology of Kozodaev et al, [23] we shall call reactions (4) multiple scattering processes. Then the relative probability of the multiple scattering of a 153-MeV π^- meson in a He^4 nucleus is

$$\gamma_{mult} = \sigma_4/(\sigma_2 + \sigma_3 + \sigma_4) = 0.29 \pm 0.06.$$

The obtained value of γ_{mult} coincides with the probability of multiple scattering in the He^4 nucleus for a pion energy of about 300 MeV [23] and is close to the probability of multiple scattering in He^4 for 630-MeV protons. [36] This fact indicates the relatively great role of multiple processes in the He^4 nucleus and that these processes are almost independent of the energy and nature of the particles.

Similarly, reaction (5) can be considered as quasi-elastic scattering of a π^- meson on a bound proton with charge exchange and reactions (6) as multiple scattering processes with charge exchange Since reactions (5) and (6) cannot be identified separately, it is impossible to determine the probability of multiple scattering with charge exchange.

An estimate of the cross section for inelastic scattering with charge exchange σ_{exc} made on the basis of the observation of two events in which the produced π^0 meson decayed by the scheme $\pi^0 \rightarrow e^- + e^+ + \gamma$ gives for σ_{exc} a value of the order 20×10^{-27} cm^2 (see Table II). Another estimate of this cross section can be made on the basis of

the relation between the cross sections for scattering of pions on free protons

$$R = Z\sigma(\pi^- + p \to \pi^0 + n) \times [Z\sigma(\pi^- + p \to \pi^- + p) + (A - Z)\sigma(\pi^+ + p \to \pi^+ + p)]^{-1}$$

under the assumption that in the case of ordinary scattering and scattering with charge exchange the influence of the nucleus is the same.[11] For pion energies $\epsilon = \epsilon_0 - V_R(\epsilon) = 170$ MeV, we have $R \approx 0.2$. Then $\sigma_{exc} \approx R\sigma_{in.sc} \approx 18$ mb.

These estimates indicate that in our case the cross section for inelastic scattering with charge exchange is approximately 10% of the inelastic cross section, which is in agreement with the results of Blinov et al.[14] In view of these data, the value $\sigma_{exc} = 62$ mb obtained by Fowler et al[22] for the π^-He interaction at 105 MeV is anomalously large and apparently erroneous.

We take this opportunity to express our deep gratitude to V. P. Dzhelepov, R. M. Sulyaev, and Yu. A. Shcherbakov for valuable discussions, to N. S. Novikova and L. A. Smirnova for programming and carrying out a number of calculations on the BÉSM and Ural computers, to L. I. Krasnoslobodtseva, T. S. Sazhneva, and Yu. D. Saĭkina for aid in the scanning and analysis of the pictures.

[1] Fernbach, Serber, and Taylor, Phys. Rev. **75**, 1352 (1949).

[2] R. Serber, Phys. Rev. **72**, 1114 (1947); M. L. Goldberger, Phys. Rev. **74**, 1269 (1948).

[3] Brueckner, Serber, and Watson, Phys. Rev. **84**, 258 (1951).

[4] Frank, Gammel, and Watson, Phys. Rev. **101**, 891 (1956).

[5] R. M. Sternheimer, Phys. Rev. **101**, 384 (1956).

[6] Bernardini, Booth, Lederman, and Tinlot, Phys. Rev. **82**, 105 (1951); Bernardini, Booth, and Lederman, Phys. Rev. **83**, 1075, 1277 (1953).

[7] Minguzzi, Puppi, and Ranzi, Nuovo cimento **11**, 697 (1954); A. Minguzzi, Nuovo cimento **12**, 799 (1954).

[8] G. E. Belovitskiĭ, JETP **35**, 838 (1958), Soviet Phys. JETP **8**, 581 (1959).

[9] Nikol'skiĭ, Kudrin, and Ali-Zade, JETP **32**, 48 (1957), Soviet Phys. JETP **5**, 93 (1957).

[10] Allen, Apostolakis, Lee, Major, and Perez Ferreira, Phil. Mag. **4**, 858 (1959).

[11] Byfield, Kessler, and Lederman, Phys. Rev, **86**, 17 (1952); J. O. Kessler and L. M. Lederman, Phys. Rev. **94**, 689 (1954).

[12] A. M. Shapiro, Phys. Rev. **84**, 1063 (1951).

[13] Dzhelepov, Ivanov, Kozodaev, Osipenkov, Petrov, and Rusakov, JETP **31**, 923 (1956), Soviet Phys. JETP **4**, 864 (1957); Ivanov, Osipenkov, Petrov, and Rusakov, JETP **37**, 863 (1959), Soviet Phys. JETP **10**, 615 (1960).

[14] Blinov, Lomanov, Shalamov, Shebanov, and Shchegolev, JETP **35**, 880 (1958), Soviet Phys. JETP **8**, 609 (1959).

[15] Wang, Wang, Ting, Dubrovskiĭ, Kladnitskaya, and Solov'ev, JETP **35**, 899 (1958), Soviet Phys. JETP **8**, 625 (1959).

[16] Kirillov-Ugryumov, Kotenko, Kuznetsov, and Sergeev, JETP **35**, 1300 (1958), Soviet Phys. JETP **8**, 907 (1959).

[17] D. H. Stork, Phys. Rev. **93**, 868 (1954).

[18] P. P. Kane, Phys. Rev. **112**, 1337 (1958).

[19] Pevsner, Rainwater, Williams, and Lindenbaum, Phys. Rev. **100**, 1419 (1955); Williams, Rainwater, and Pevsner, Phys. Rev. **101**, 412 (1956); Williams, Baker, and Rainwater, Phys. Rev. **104**, 1695 (1956); Baker, Rainwater, and Williams, Phys. Rev. **112**, 1763 (1958); Baker, Byfield, and Rainwater, Phys. Rev. **112**, 1773 (1958); Edelstein, Baker, and Rainwater, Phys. Rev. **122**, 252 (1961).

[20] L. S. Kisslinger, Phys. Rev. **98**, 761 (1955).

[21] T. A. Fujii, Phys. Rev. **113**, 695 (1959).

[22] Fowler, Fowler, Shutt, Thorndike, and Whittemore, Phys. Rev. **91**, 135 (1953).

[23] Kozodaev, Sulyaev, Filippov, and Shcherbakov, JETP **31**, 701 (1956), Soviet Phys. JETP **4**, 580 (1957); JETP **33**, 1047 (1957), Soviet Phys. JETP **6**, 806 (1958); Kozodaev, Kulyukin, Sulyaev, Filippov, and Shcherbakov, JETP **38**, 409 (1960), Soviet Phys. JETP **11**, 300 (1960); JETP **39**, 929 (1960), Soviet Phys. JETP **12**, 644 (1961).

[24] Brautti, Chersovani, Franzinetti, Sedmak-Furlan, and Tosi-Torelli, Nuovo cimento **19**, 1270 (1961).

[25] Budagov, Viktor, Dzhelepov, Ermolov, and Moskalev, JETP **38**, 734 (1960), Soviet Phys. JETP **11**, 531 (1960); Nuclear Phys. **22**, 226 (1961).

[26] Budagov, Ermolov, Kushnirenko, and Moskalev, JETP **40**, 1615 (1961), Soviet Phys. JETP **13**, 1136 (1961).

[27] Budagov, Viktor, Dzhelepov, Ermolov, and Moskalev, JETP **38**, 1047 (1960), Soviet Phys. JETP **11**, 755 (1960).

[28] Ignatenko, Mukhin, Ozerov, and Pontecorvo, DAN SSSR **103**, 209 (1955); JETP **31**, 546 (1956), Soviet Phys. JETP **4**, 351 (1957).

[29] L. Infeld, Quart. Appl. Math. **5**, 113 (1947); A. L. Aden, J. Appl. Phys. **22**, 601 (1951).

[30] L. I. Schiff, Quantum Mechanics, McGraw-Hill, 1949 (Russ. Transl. IIL, M. 1957), Chap. 7.

[31] Bloch, Hull, Broyles, Bouricius, Freeman, and Breit, Revs. Modern Phys. **23**, 147 (1951).

[32] R. D. Woods and D. S. Saxon, Phys. Rev. **95**, 577 (1954).

[33] Goldberger, Miyazawa, and Oehme, Phys. Rev. **99**, 986 (1955).
[34] Ashkin, Blaser, Feiner, and Stern, Phys. Rev. **101**, 1149 (1956).
[35] K. M. Watson and C. Zemach, Nuovo cimento **10**, 452 (1958).
[36] Kozodaev, Kulyukin, Sulyaev, Filippov, and Shcherbakov, JETP **38**, 708 (1960), Soviet Phys. JETP **11**, 511 (1960).

Translated by E. Marquit
198